

# Phase-field simulation of magnetoelastic couplings in ferromagnetic shape memory alloys

L.J. Li<sup>a</sup>, C.H. Lei<sup>a</sup>, Y.C. Shu<sup>b</sup>, J.Y. Li<sup>a,\*</sup>

<sup>a</sup> Department of Mechanical Engineering, University of Washington, Seattle, WA 98195-2600, USA

<sup>b</sup> Institute of Applied Mechanics, National Taiwan University, Taipei 106, Taiwan, ROC

Received 17 October 2010; received in revised form 24 December 2010; accepted 2 January 2011

## Abstract

Ferromagnetic shape memory alloys (FSMAs) possess coupled ferroelastic and ferromagnetic orderings simultaneously, making it possible to manipulate ferroelastic twins of FSMAs via a magnetic field or magnetic domains via mechanical loading. In this paper, we develop a phase-field model to simulate the formation and evolution of magnetoelastic domains in FSMAs under combined mechanical and magnetic loadings, taking into account both variant rearrangement and magnetization rotation. It is found that the large magnetic field induced strain in FSMAs results from a variant rearrangement process, yet such variant rearrangement can be blocked by a relatively large compressive stress, substantially reducing the magnetic field induced strain. Furthermore, either pseudoelastic or quasi-plastic behavior is exhibited in FSMAs subjected to varying compressive stress, depending on the strength of the constant magnetic field applied. These results agree well with experiments, and can be used to guide the design and optimization of FSMAs.

© 2011 Acta Materialia Inc. Published by Elsevier Ltd. All rights reserved.

**Keywords:** Ferromagnetic shape memory alloys; Phase-field simulation; Magnetic domains; Magnetoelasticity

## 1. Introduction

Ferromagnetic shape memory alloys (FSMAs) possess both ferroelastic and ferromagnetic orderings simultaneously; these orderings are coupled together, making it possible to manipulate ferroelastic twins of FSMAs via a magnetic field or magnetic domains via mechanical loading. Such magnetoelastic couplings render FSMAs attractive for rapidly responding magnetic sensing and actuation [1–7], and, indeed, magnetic field induced strain as high as 10% has been demonstrated [8]. While many experimental investigations have focused on NiMnGa alloys [6,9,10], ferromagnetic shape memory effects have also been observed in many other material systems that usually exhibit smaller magnetic field induced strain, including FePd [2], FePt [11], NiCoGa [12], NiCoAl [7], NiFeGa [13] and NiCoMnIn [14].

The microstructural mechanism responsible for the large magnetic field induced strain in FSMAs is well understood [2,6,9,15–24], and such a giant strain is achieved mainly through reorientation of ferroelastic variants induced by a magnetic field. However, the details of microstructure evolution in FSMAs are less clear. In fact, there are two mechanisms of microstructure evolution in FSMAs, one through the rearrangement of ferroelastic variants, and the other through the rotation of magnetization. While the reorientation of ferroelastic variants in FSMAs has been extensively investigated [2,21,22,25–27], the significance of magnetization rotation has only recently been recognized [28,29]. In particular, it has been noted that magnetization rotation is no longer negligible under a relatively large compressive stress, which has significant effect on the magnetoelastic behavior of FSMAs [28,29]. Indeed, a relatively large constant compressive stress of 3 MPa blocked the rearrangement of ferroelastic variants in a NiMnGa crystal, resulting in a much smaller magnetic field induced strain being observed experimentally [9]. A related

\* Corresponding author. Tel.: +1 206 543 6226; fax: +1 206 685 8047.  
E-mail address: [jjli@u.washington.edu](mailto:jjli@u.washington.edu) (J.Y. Li).

phenomenon is the stress–strain response of FSMAs subjected to a constant magnetic field, wherein either pseudo-elastic or quasiplastic behavior is exhibited, depending on the strength of the applied magnetic field [9,30–32]. Both of these phenomena are closely related to the microstructure evolutions of FSMAs, and have significant implications to their practical applications. The goal of this work is thus to investigate numerically the process of variant rearrangement and magnetization rotation in FSMAs subjected to combined mechanical and magnetic loading through phase-field simulations, with the objective of guiding the design and optimization of FSMAs with higher blocking stress and energy density.

Several theoretical models have already been developed to predict the magnetic field induced strain in FSMAs [2,10,21–23,25–28,30,33–42]; most of these are based on the minimization of the total free energy of the system. A conventional phase-field method has also been developed to simulate the microstructures of FSMAs and their interactions [20,43–46], based on magnetoelastic energy expanded in terms of the polynomial of magnetization and transformation strain. This requires fine tuning of many expansion coefficients to yield correct symmetries and energy wells of FSMAs, wherein the coupling between magnetic and ferroelastic orderings is not always straightforward. We seek to overcome these difficulties in this work.

Our approach is based on a phase-field model with an explicit energy well structure that substantially simplifies the computational study of domain structures and their evolution in phase-transforming materials [47–55]. It is much easier to implement couplings among multiple order parameters using this approach, and thus it is particularly suitable for studying FSMAs. Some of our preliminary results have been reported in a short letter [53] and here we systematically present our theory and results in detail.

## 2. Theoretical framework

### 2.1. Energetics

Two order parameters, transformation strain and magnetization, are required to describe the state of FSMAs, and they are usually coupled, such that the easy axis of the magnetization is aligned along a particular crystalline axis of transformation strain. To appreciate this, we consider a single-crystalline FSMA with tetragonal symmetry, for which a total of three ferroelastic variants exist as schematically shown in Fig. 1, with their transformation strain given by:

$$\boldsymbol{\varepsilon}^{(1)} = \begin{pmatrix} \beta & 0 & 0 \\ 0 & \xi & 0 \\ 0 & 0 & \xi \end{pmatrix}, \boldsymbol{\varepsilon}^{(2)} = \begin{pmatrix} \xi & 0 & 0 \\ 0 & \beta & 0 \\ 0 & 0 & \xi \end{pmatrix}, \boldsymbol{\varepsilon}^{(3)} = \begin{pmatrix} \xi & 0 & 0 \\ 0 & \xi & 0 \\ 0 & 0 & \beta \end{pmatrix}, \quad (1)$$

where  $\xi$  and  $\beta$  are components of the tetragonal transformation strain that can be determined from lattice parameters of FSMAs. Notice that in each of the variants, the

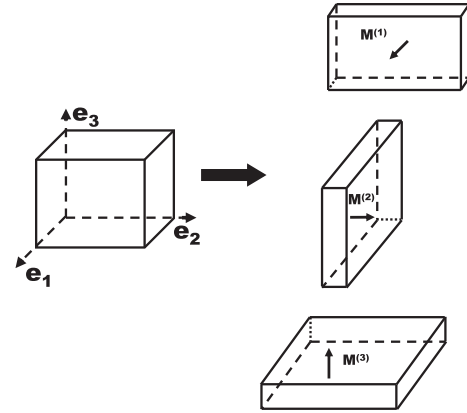


Fig. 1. Schematics of three ferroelastic variants with distinct transformation strain (represented by shortening along one axis of the cubic lattice and elongation along the other two axes); the magnetic easy axis is denoted by a solid arrow along the unique axis of the ferroelastic variant.

magnetization  $\mathbf{M}$  tends to be aligned along the unique tetragonal axis of the transformation strain, and this coupling makes it possible to manipulate the transformation strain by a magnetic field, or the magnetization by mechanical loading.

In conventional phenomenological theory, the internal energy density of FSMAs is expanded in terms of the polynomial of magnetization and transformation strain [20,43,46,56]. This results in many expansion coefficients that need to be carefully tuned to yield correct symmetry and energy wells, and the couplings among different order parameters are not often straightforward. To overcome these difficulties, we notice that the transformation strain of FSMAs at any particular spatial point can be expressed in terms of the characteristic function of variants and their corresponding transformation strain:

$$\boldsymbol{\varepsilon}^* = \lambda_1 \boldsymbol{\varepsilon}^{(1)} + \lambda_2 \boldsymbol{\varepsilon}^{(2)} + \lambda_3 \boldsymbol{\varepsilon}^{(3)}, \quad (2)$$

where  $\lambda_i(\mathbf{x})$  is the characteristic function of variant  $i$ , which is specified as:

$$\lambda_i(\mathbf{x}) = \begin{cases} 1, & \mathbf{x} \text{ occupied by variant } i \\ 0, & \text{otherwise} \end{cases}. \quad (3)$$

For tetragonal FSMAs, there are a total of three  $\lambda_i(\mathbf{x})$  for three ferroelastic variants, but only two of them are independent, subject to the following constraint:

$$\lambda_1 + \lambda_2 + \lambda_3 = 1, \quad (4)$$

so that any spatial point  $\mathbf{x}$  is occupied, and only occupied by one variant. To incorporate this constraint, we introduce two independent variables,  $\mu_1$  and  $\mu_2$ , that are either 0 or 1, and let:

$$\lambda_1 = \mu_1, \quad \lambda_2 = (1 - \mu_1)\mu_2, \quad \lambda_3 = (1 - \mu_1)(1 - \mu_2), \quad (5)$$

so that Eq. (4) is satisfied automatically. This establishes the equivalence of characteristic functions  $\boldsymbol{\mu} = \{\mu_1, \mu_2\}$  with the transformation strain  $\boldsymbol{\varepsilon}^*$ , and can be interpreted as multi-rank laminations that are proven to minimize the energy of martensitic phase transformation [57], magnetic materi-

als [34] and ferroelectrics [58,59]. This approach allows us to use  $\mu_1$  and  $\mu_2$  as the internal variables to describe the ferroelastic state instead, and to make sure that  $\mu_i$  takes either 0 or 1, the following energy penalty is proposed:

$$W_s^{ani} = K_s \sum_{i=1}^2 \mu_i^2 (1 - \mu_i)^2, \quad (6)$$

which is minimized by  $\mu_i = 0$  or 1.

For each of the ferroelastic variants, the magnetic easy axis is aligned along the unique axis of the tetragonal transformation strain, which can be specified using the characteristic functions  $\mathbf{l}_i$  as:

$$\mathbf{I}(\boldsymbol{\mu}) = \lambda_1 \mathbf{l}^{(1)} + \lambda_2 \mathbf{l}^{(2)} + \lambda_3 \mathbf{l}^{(3)}, \quad (7)$$

where the easy axis  $\mathbf{l}^{(i)}$  of each individual variant is given by:

$$\mathbf{l}^{(1)} = \begin{pmatrix} 1 \\ 0 \\ 0 \end{pmatrix}, \quad \mathbf{l}^{(2)} = \begin{pmatrix} 0 \\ 1 \\ 0 \end{pmatrix}, \quad \mathbf{l}^{(3)} = \begin{pmatrix} 0 \\ 0 \\ 1 \end{pmatrix}. \quad (8)$$

This explicitly couples the ferroelastic ordering  $\boldsymbol{\mu}$  and ferromagnetic ordering  $\mathbf{m}(\mathbf{x}) = \frac{1}{M_s} \mathbf{M}(\mathbf{x})$ , where  $M_s$  is the saturation magnetization. In particular, when the magnetization rotates away from the easy axis, magnetic anisotropy energy results:

$$W_m^{ani} = K_u [1 - (\mathbf{m} \cdot \mathbf{I}(\boldsymbol{\mu}))^2], \quad (9)$$

which is minimized when the magnetization is aligned along the easy axis. In addition, such magnetization rotation also leads to magnetostrictive strain given by:

$$\boldsymbol{\varepsilon}^m(\mathbf{m}) = \frac{3}{2} [\gamma_1 \mathbf{m} \otimes \mathbf{m} + \gamma_2 \sum_{i \neq l} m_i m_l (\mathbf{k}_i \otimes \mathbf{k}_l)], \quad (10)$$

where  $\gamma_1$  and  $\gamma_2$  are magnetostrictive constants,  $\{\mathbf{k}_1, \mathbf{k}_2, \mathbf{k}_3\}$  is the orthonormal basis parallel to the cubic axes, and  $m_i = \mathbf{m} \cdot \mathbf{k}_i$  are the direction cosines of the magnetization. As such, the inelastic strain of FSMAs consists of both transformation strain and magnetostrictive strain, and the elastic energy density of FSMAs is given by:

$$W^{elas} = \frac{1}{2} [\boldsymbol{\varepsilon} - \boldsymbol{\varepsilon}^*(\boldsymbol{\mu}) - \boldsymbol{\varepsilon}^m(\mathbf{m})] \cdot \mathbf{C} [\boldsymbol{\varepsilon} - \boldsymbol{\varepsilon}^*(\boldsymbol{\mu}) - \boldsymbol{\varepsilon}^m(\mathbf{m})], \quad (11)$$

where  $\mathbf{C}$  is the elastic stiffness and  $\boldsymbol{\varepsilon}$  is the total strain, which can be determined by solving mechanical equilibrium equation [47,48,53,55].

Now consider a FSMA specimen occupying a region  $\Omega$  and subjected to an external stress  $\boldsymbol{\sigma}^0$  and an magnetic field  $\mathbf{H}^0$ . The potential energy of the system can be described as [28,53,60]:

$$\begin{aligned} \mathcal{J}(\boldsymbol{\mu}, \mathbf{m}) = & \int_{\Omega} \{ W^{int}(\nabla \boldsymbol{\mu}, \nabla \mathbf{m}) + W_s^{ani}(\boldsymbol{\mu}) + W_m^{ani}(\boldsymbol{\mu}, \mathbf{m}) \\ & + W^{elas}(\boldsymbol{\mu}, \mathbf{m}) - \boldsymbol{\sigma}^0 \cdot \boldsymbol{\varepsilon} - \mu_0 \mathbf{H}^0 \cdot \mathbf{M} \} d\mathbf{x} \\ & + \frac{\mu_0}{2} \int_{\mathbb{R}^3} |\nabla \phi|^2 d\mathbf{x}. \end{aligned} \quad (12)$$

In addition to the energetic contributions already discussed, we also have:

$$W^{int} = A_1 |\nabla \boldsymbol{\mu}|^2 + A_2 |\nabla \mathbf{m}|^2, \quad (13)$$

which accounts for the interfacial energy of domain walls, with the first term describing the ferroelastic domain wall energy penalizing the gradient in  $\boldsymbol{\mu}$ , and the second term describing the magnetic domain wall energy penalizing the gradient in  $\mathbf{m}$ . Furthermore the magnetostatic energy arising from the magnetization distribution in FSMAs has to be considered, with the magnetic potential  $\phi$  solved from Maxwell's equations, and  $\mu_0 = 4\pi \times 10^{-7} \text{N/A}^2$  being the permeability of free space. The work done by the external stress and the magnetic field are also subtracted.

## 2.2. Kinetics

Under an external magnetic or mechanical loading, both  $\boldsymbol{\mu}$  and  $\mathbf{m}$  will evolve to minimize the potential energy  $\mathcal{J}$ . The variation of the potential energy  $\mathcal{J}$  with respect to  $\boldsymbol{\mu}$  and  $\mathbf{m}$  under a periodic boundary condition is derived as: [48,55]

$$\begin{aligned} \delta \mathcal{J}(\boldsymbol{\mu}, \mathbf{m}) = & - \int_{\Omega} (\mathbf{F}_{\boldsymbol{\mu}}^{int} + \mathbf{F}_{\boldsymbol{\mu}}^{ani} + \mathbf{F}_{\boldsymbol{\mu}}^{ela} + \mathbf{F}_{\mathbf{m}}^{ani}) \cdot \delta \boldsymbol{\mu} dV - \mu_0 M_s \\ & \times \int_{\Omega} (\mathbf{H}^{int} + \mathbf{H}^{ani} + \mathbf{H}^{elas} + \mathbf{H}^0 + \mathbf{H}^d) \cdot \delta \mathbf{m} dV, \end{aligned} \quad (14)$$

with the driving forces for the evolution of characteristic function  $\boldsymbol{\mu}$  given by:

$$\begin{aligned} \mathbf{F}_{\boldsymbol{\mu}}^{int} &= 2A_1 \nabla^2 \boldsymbol{\mu}, \\ \mathbf{F}_{\boldsymbol{\mu}}^{ani} &= - \frac{\partial}{\partial \boldsymbol{\mu}} W_s^{ani}(\boldsymbol{\mu}), \\ \mathbf{F}_{\mathbf{m}}^{ani} &= - \frac{\partial}{\partial \boldsymbol{\mu}} W_m^{ani}(\boldsymbol{\mu}, \mathbf{m}), \\ \mathbf{F}_{\boldsymbol{\mu}}^{elas} &= \mathbf{C} [\boldsymbol{\varepsilon} - \boldsymbol{\varepsilon}^*(\boldsymbol{\mu}) - \boldsymbol{\varepsilon}^m(\mathbf{m})] \cdot \frac{\partial \boldsymbol{\varepsilon}^*(\boldsymbol{\mu})}{\partial \boldsymbol{\mu}}, \end{aligned} \quad (15)$$

and the effective fields that drive the evolution of magnetization  $\mathbf{m}$  given by:

$$\begin{aligned} \mathbf{H}^{int} &= \frac{2A_2}{\mu_0 M_s} \nabla^2 \mathbf{m}, \\ \mathbf{H}^{ani} &= - \frac{1}{\mu_0 M_s} \frac{\partial}{\partial \mathbf{m}} W_m^{ani}(\boldsymbol{\mu}, \mathbf{m}), \\ \mathbf{H}^{elas} &= \frac{1}{\mu_0 M_s} \mathbf{C} [\boldsymbol{\varepsilon} - \boldsymbol{\varepsilon}^*(\boldsymbol{\mu}) - \boldsymbol{\varepsilon}^m(\mathbf{m})] \cdot \frac{\partial \boldsymbol{\varepsilon}^m(\mathbf{m})}{\partial \mathbf{m}}, \\ \mathbf{H}^d &= -\nabla \phi. \end{aligned} \quad (16)$$

Assuming linear kinetics, the evolution equation governing the field variable  $\boldsymbol{\mu}$  can be derived as:

$$\frac{\partial \boldsymbol{\mu}}{\partial t} = L [\mathbf{F}_{\boldsymbol{\mu}}^{int} + \mathbf{F}_{\boldsymbol{\mu}}^{ani} + \mathbf{F}_{\boldsymbol{\mu}}^{ela} + \mathbf{F}_{\mathbf{m}}^{ani}], \quad (17)$$

with  $L$  being the evolution coefficient, while the rotation of magnetization is described by the Landau–Lifschitz–Gilbert (LLG) equation: [20,45,61–63],

$$\frac{\partial \mathbf{m}}{\partial t} = -\gamma_g \mathbf{m} \times \mathbf{H}^{\text{eff}} - \delta \gamma_g \mathbf{m} \times (\mathbf{m} \times \mathbf{H}^{\text{eff}}), \quad (18)$$

where  $\gamma_g \approx 2.21 \times 10^5 \text{ mA}^{-1} \text{ s}^{-1}$  is the gyromagnetic ratio and  $\delta$  is the dimensionless damping coefficient. Clearly, the variant rearrangement process in FSMAs is described by the evolution Eq. (17), while its magnetization rotation process is described by the evolution Eq. (18), and both mechanisms for microstructure evolution are accounted for in this framework. In addition, these two processes are coupled together through the driving forces and effective fields given in Eqs. (15) and (16).

### 3. Results and discussion

The equations governing the evolution of  $\boldsymbol{\mu}$  and  $\mathbf{m}$  have been solved using a semi-implicit finite-difference scheme on the time scale and the Fourier transform method on the spatial scale [48,55,56], and have been implemented to simulate the microstructure evolution and macroscopic response of  $\text{Ni}_2\text{MnGa}$  crystal, with the material constants used in the simulation listed in Table 1 [9,15,21,28]. The representative ferroelastic and magnetic domain structures as well as their evolutions under combined mechanical and magnetic loadings are investigated, as summarized in the following subsections.

#### 3.1. Magnetoelastic domains under different constraints

We first consider the formation of magnetoelastic domains in a FSMA subjected to different constraints, as shown in Fig. 2. Under a clamped boundary condition where no deformation is allowed, a self-accommodating domain structure emerges, as shown in Fig. 2a, consisting of two ferroelastic variants 1 and 3 of equal volume fractions, separated by 90 degree domain walls along the  $(10\bar{1})$  plane. Furthermore, each of the ferroelastic twins is divided into two different magnetic domains separated by 180 degree domain walls along the  $(100)$  or  $(001)$  planes, resulting in a rank-2 laminated domain structure as predicted by the constrained theory [2,23]. This is in excellent agreement with the experimentally observed domain structure, as shown in Fig. 2b. If a large magnetic field is applied along the  $[001]$  axis to this clamped domain structure, then it is observed that magnetization in ferroelastic variant 1 rotates away from its easy axis along  $[100]$  to the direction of the applied field, resulting in a uniform distribution of magnetization over two different ferroelastic variants, as shown in Fig. 2c. On the other hand, if a compressive stress is applied along the  $[100]$  axis with clamped boundary condition removed, a single ferroelastic variant 1 consists of two magnetic domains separated by

180 degree domain wall emerges, as shown in Fig. 2d. This is close to the initial condition of a FSMA specimen subjected to constant compressive stress and a varying magnetic field perpendicular to it, which we will investigate next. Note that a uniform magnetization distributed over a single ferroelastic variant will emerge from the simulation under a large magnetic field without clamped boundary condition, though it is not presented here. These results suggest that the microstructure of FSMAs is indeed sensitive to the applied mechanical and magnetic loadings, and thus can be manipulated accordingly.

#### 3.2. Magnetic field induced evolution under constant compressive stress

We now consider a typical experimental configuration [9,28], where a FSMA rod is subjected to a constant compressive stress  $\boldsymbol{\sigma}^0$  along the longer axis of the rod parallel to the  $[100]$  axis of the crystal, while a varying magnetic field  $\mathbf{H}^0$  is applied parallel to its  $[001]$  axis. As indicated earlier, a rank-1 laminated domain structure with equal volume fractions of 180 degree magnetic domains similar to that in Fig. 2d is used as the initial configuration, with a single layer of variant 3 less than 1% of the total volume added to facilitate nucleation, as often observed in experiments [31] and adopted in computations [64,65]. The resulting magnetoelastic responses of a FSMA under three different stress magnitudes are shown in Fig. 3, along with experimental data. It is observed that the magnitude of compressive stress has a significant effect on the axial strain and magnetization, as shown in Fig. 3a, in excellent agreement with experimental measurements. A close examination reveals that as the magnetic field along the  $[001]$  axis increases, either variant rearrangement or magnetization rotation will dominate evolution of the domain structure, depending on the magnitude of the applied compressive stress. For example, when a small compressive stress of 0.6 MPa is applied, small magnetization rotation occurs first, but variant rearrangement quickly takes over as the dominant evolution mechanism, leading to a large jump in magnetic field induced strain at 0.3 T and correspondingly a larger slope of the magnetization curve, as shown by the broken blue curve in Fig. 3a and b, which agrees very well with experimental data [9]. To appreciate this, we also present the intermediate domain structure before the saturation of magnetization, as shown in Fig. 3c, which reveals a very characteristic rank-2 laminated domain structure, where variant 3 is observed to grow at the expense of variant 1, which are separated by a 90 degree domain wall along  $(\bar{1}01)$  plane. A small magnetization rotation is indeed observed in variant 1, consistent with Ma and Li's analysis [28,29]. On the other hand, when a relatively large compressive stress of 3 MPa is applied, the variant rearrangement process is completely blocked, leading to magnetostrictive strain that is orders of magnitude smaller than transformation strain, as shown by the solid soft blue curve in Fig. 3a, also in excellent agreement with experi-

Table 1  
Material parameters of  $\text{Ni}_2\text{MnGa}$ .

$K_s$ ( $\text{J m}^{-3}$ )	$K_u$ ( $\text{J m}^{-3}$ )	$M_s$ (T)	$E$ (Gpa)	$\nu$	$\xi$	$\beta$
$1.65 \times 10^5$	$1.65 \times 10^5$	0.63	154	0.3	0.021	-0.034

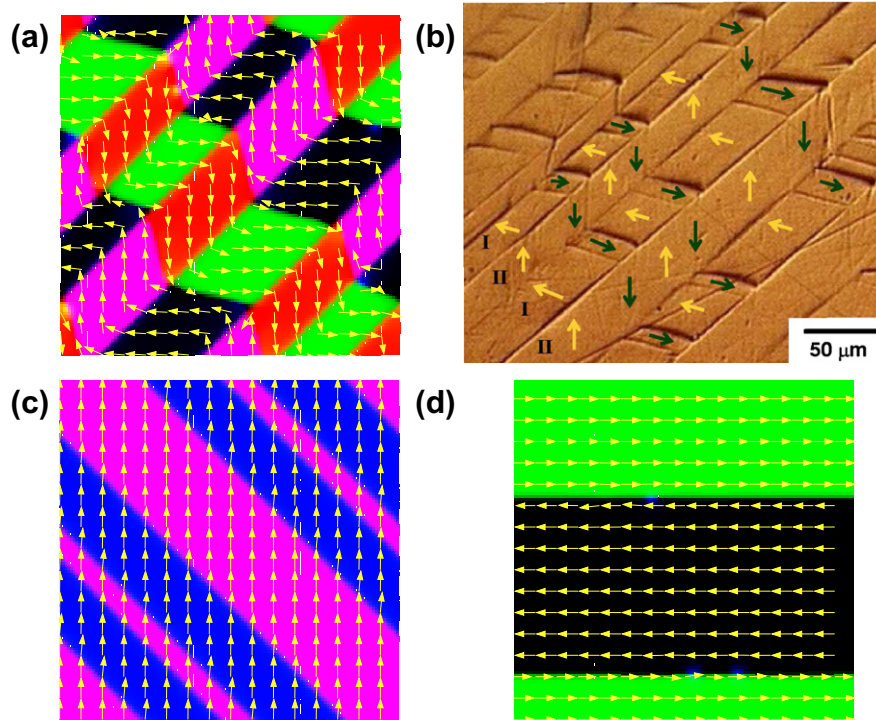


Fig. 2. The formation of magnetoelastic domains in a FSMA: (a) rank-2 laminated domain pattern under a clamped BC; (b) the experimentally observed domain structure of the FSMA [24]; (c) uniform magnetization distribution over two ferroelastic twins under clamped BC and a magnetic field; (d) a single ferroelastic variant 1 consists of two magnetic domains separated by 180 degree domain wall under stressed BC; the colors green, black and blue are used to indicate variant 1, while fuchsia and red are used to indicate variant 3; the arrow indicates the direction of magnetization along with the different colors. (For interpretation of the references to color in this figure legend, the reader is referred to the web version of this article.)

ment [9]. No change in the slope of the magnetization curve is observed before saturation in Fig. 3b, another indication of magnetization rotation instead of variant rearrangement, again in good agreement with experiment [9]. Examination of the intermediate domain structure before magnetization saturation reveals that  $\mu$  is indeed unchanged throughout the magnetization process, and only magnetization rotation occurs, as shown in Fig. 3d, where a rank-1 laminate is observed with identical  $\mu$  but different magnetization directions. When a modest external stress of 1.4 MPa is applied, the axial strain and magnetization curves are very similar to those under 0.6 MPa. However, the calculated saturation strain is larger than the experimental value, probably because the single-variant state has not been reached in the experiment. Note that all the conditions in these three simulations are identical except the magnitude of the applied compressive stress.

### 3.3. Stress-induced evolution under a constant magnetic field

We then consider a  $\text{Ni}_2\text{MnGa}$  rod subjected to a constant magnetic field  $\mathbf{H}^0$  parallel to the [001] axis and a varying compressive stress  $\sigma^0$  along the [100] axis of the crystal. Unless otherwise noted, a single variant 3 with a uniform magnetization distribution is used as the initial condition, with a single layer of variant 1 less than 1% of total volume added to facilitate nucleation. The resulting stress–strain

curves and demagnetization curves under three different magnitudes of magnetic field are shown in Fig. 4, which shows excellent agreement with the experimental data. The loading portion of the stress–strain curves are very similar, regardless of the strength of the magnetic field, as seen in Fig. 4a, where the initial linear elastic deformation is quickly taken over by a gradual plateau wherein large axial strain is observed with a small increase in stress, indicating the process of variant rearrangement triggered by increased compressive stress that favors variant 1 over variant 3. The plateau is lower for FSMAs under a smaller magnetic field, since smaller stress is required to overcome the applied magnetic field. After the strain is saturated at approximately 6%, a sharp increase in stress is observed, regardless of applied magnetic field, indicating elastic deformation on a single variant after the completion of the variant rearrangement process. The unloading response, however, is quite different for different curves. Either pseudoelastic or quasiplastic behavior is exhibited, depending on the strength of the applied magnetic field. Under a small magnetic field, for example 0 T, quasiplastic behavior is observed, and the axial strain is not recovered after removal of stress, due to the lack of a restoring magnetic field. A large magnetic field of 0.9 T, on the other hand, results in a pseudoelastic behavior where the axial strain is completely recovered after unloading. For an intermediate magnetic field of 0.5 T, only part of the axial strain is recovered. Furthermore, the applied compressive

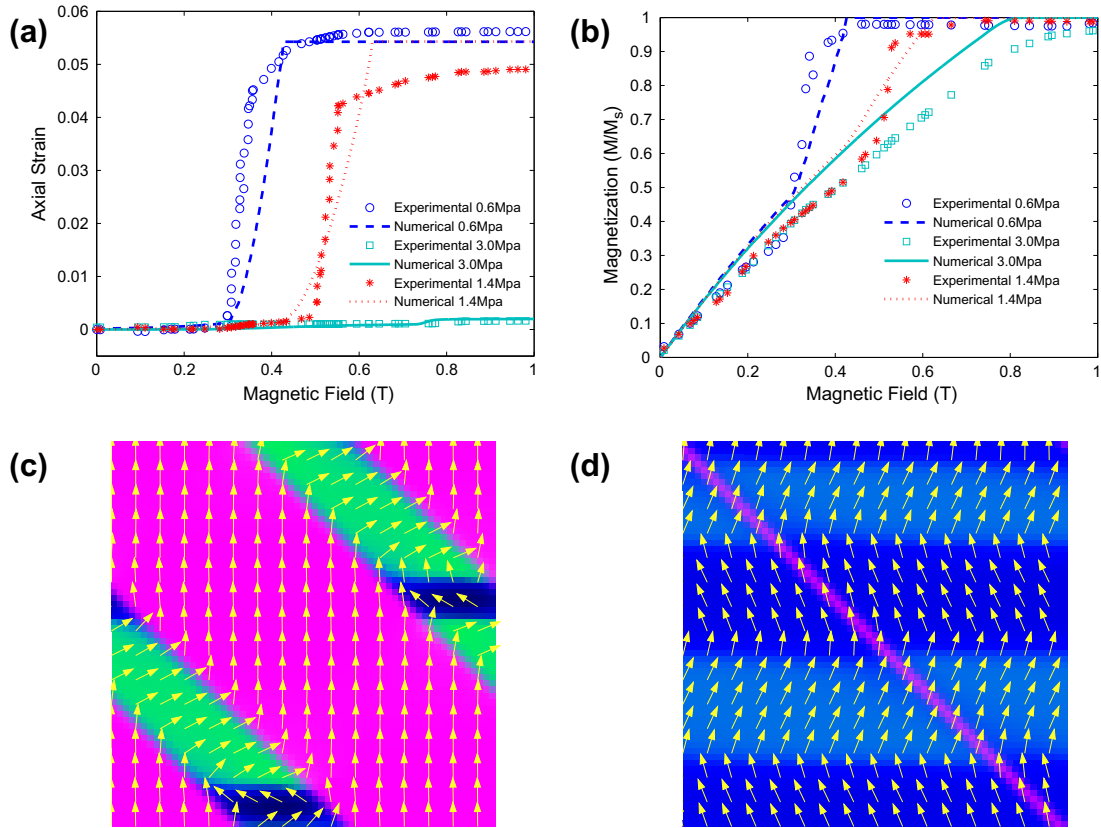


Fig. 3. The magnetic field induced evolution of a FSMA under a constant compressive stress: (a) axial strain and (b) magnetization vs. the applied magnetic field under compressive axial stress of  $\sigma^0 = 0.6, 1.4$  and  $3$  MPa, respectively; the experimental data is taken from Ref. [9]; the magnetoelastic domains at an intermediate stage of magnetization under different compressive stresses of (c)  $0.6$  MPa and (d)  $3.0$  MPa are given below; green and blue are used to indicate variant 1, while fuchsia is used to indicate variant 3; the arrow indicates the direction of magnetization. (For interpretation of the references to color in this figure legend, the reader is referred to the web version of this article.)

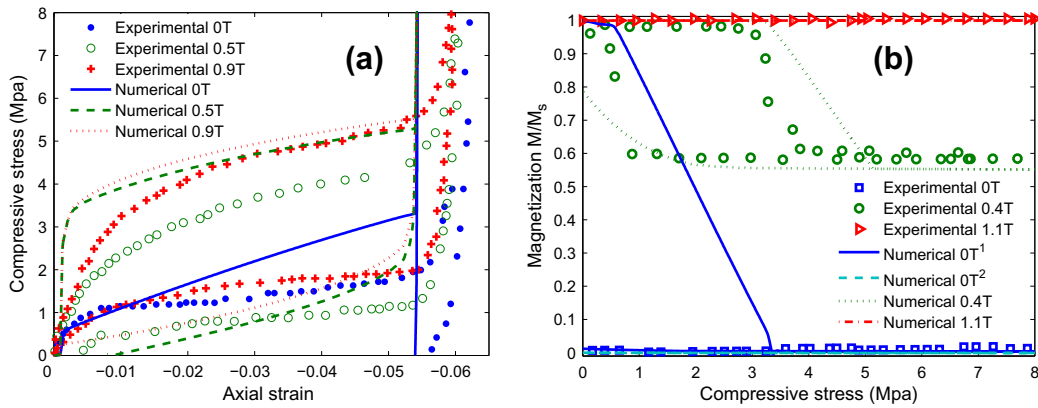


Fig. 4. The stress-induced evolution in a FSMA under constant magnetic field: (a) the stress–strain curves under magnetic fields of  $0, 0.5$  and  $0.9$  T, respectively; (b) the demagnetization curve under magnetic fields of  $0, 0.4$  and  $1.1$  T, respectively, with the curve marked as  $0\text{ T}^2$  achieved from the initial configuration shown in Fig. 2d. The experimental data are taken from Refs. [31,9].

stress also tends to demagnetize the FSMA, as shown in Fig. 4b. Under a small magnetic field such as  $0$  T, the FSMA is easily demagnetized by the compressive stress, and after unloading, the magnetization is not recovered, as shown by the solid blue curve in Fig. 4b. On the other hand, when a large magnetic field of  $1.1$  T is applied, the demagnetization is totally blocked, resulting in an unchanged saturation

magnetization along the  $[001]$  direction during the entire evolution process, as shown by the red dot-dashed curve in Fig. 4b. When a modest magnetic field, e.g.  $0.4$  T, is applied, the demagnetization effect of stress is partially balanced by the applied magnetic field, and the FSMA is not fully demagnetized by the stress. After the unloading of the compressive stress, the magnetization will recover to

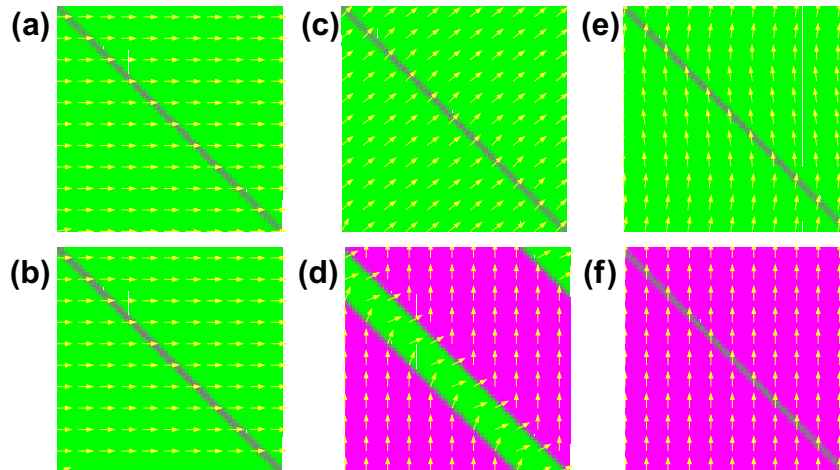


Fig. 5. The magnetoelastic domains of a FSMA after loading (first row) and unloading (second row) by a varying compressive stress, with a constant magnetic field of 0 T (a, b), 0.5 T (c, d), and 0.9 T (e, f) applied; the maximum compressive stress applied is  $\sigma^0 = 8.0$  MPa; the color green is used to indicate variant 1, while fuchsia used to indicate variant 3; the arrow indicates the magnetization direction. (For interpretation of the references to color in this figure legend, the reader is referred to the web version of this article.)

its original state. If the initial condition is similar to those given in Fig. 2d instead, and no magnetic field is applied, then the magnetization remains flat throughout the process, as shown in the curve marked by 0 T<sup>2</sup>. Excellent agreement with experimental data is observed for all these cases.

To fully understand the differences in stress–strain curves and demagnetization curves under different magnetic field, we examine the configuration of magnetoelastic domains under different magnetic fields, as shown in Fig. 5. The first row shows the magnetoelastic domains after loading to maximum compressive stress, where it is observed that variant 3 is completely converted to variant 1 by the compressive stress, regardless of magnetic field. The magnetization distribution, however, is quite different. When no magnetic field is applied, the magnetization is aligned along the easy axis of variant 1, and the FSMA is completely demagnetized from its original magnetization direction, as shown in Fig. 5a. Under a large magnetic field of 0.9 T, the magnetization is unchanged from its original direction, and the magnetization rotation process is completely blocked, as seen in Fig. 5e. The magnetization direction under a modest field of 0.5 T is between the easy axis of variant 1 and the original magnetization direction, so it is demagnetized by the compressive stress to some extent, but not completely, consistent with what we observed in Fig. 4b. After unloading of the compressive stress, the corresponding magnetoelastic domains are shown in the second row of Fig. 5. When no magnetic field is applied, the domains after unloading are unchanged from the domains at maximum loading of compressive stress, as shown in Fig. 5b, suggesting that neither axial strain nor magnetization will be recovered after the unloading. Under a large magnetic field of 0.9 T, however, variant 1 is converted back to variant 3, suggesting that both axial strain and magnetization will be fully recovered, consistent with what we observed in Fig. 4. When a modest magnetic field of 0.5 T is applied, then variant 1 is largely converted back

to variant 3, though some residual variant 1 remains, suggesting that neither axial strain nor magnetization are fully recovered. The simulations thus offer insight into the detailed microstructure evolution process in FSMAs.

#### 4. Summary

In summary, we have developed a phase-field model of FSMAs with coupled ferroelastic and ferromagnetic orderings, and have used it to simulate the formation and evolution of magnetoelastic domains under combined mechanical and magnetic loadings; we have also studied the implications of these domains for the macroscopic responses of FSMAs. Excellent agreements with experimental data are observed.

#### Acknowledgements

We gratefully acknowledge the support of US ARO (W911NF-07-1-0410) and NSF (DMR-0706100 and DMR-1006194). Shu is also supported by TW NSC (97-2221-E-002 -125 -MY3).

#### References

- [1] Ullakko K, Huang JK, Kantner C, O'Handley RC, Kokorin VV. *Appl Phys Lett* 1996;69:1966.
- [2] James RD, Wuttig M. *Philos Mag A* 1998;77:1273.
- [3] James RD, Tickle R, Wuttig M. *Mat Sci Eng A – Struct* 1999;273:275:320.
- [4] Tickle R, James RD. *J Magn Magn Mater* 1999;195:627.
- [5] Murray SJ, Marioni M, Allen SM, O'Handley RC, Lograsso TA. *Appl Phys Lett* 2000;77:886.
- [6] Heczko O, Sozinov A, Ullakko K. *IEEE Trans Magn* 2000;36:3266.
- [7] Oikawa K, Ota T, Gejima F, Ohmori T, Kainuma R, Ishida K. *Mater Trans* 2001;42:2472.
- [8] Sozinov A, Likhachev AA, Lanska N, Ullakko K. *Appl Phys Lett* 2002;80:1746.
- [9] Heczko O. *J Magn Magn Mater* 2005;290:787–94.

- [10] Heczko O, Straka L, Hannula SP. *Mat Sci Eng A – Struct* 2006;438:1003.
- [11] Kakeshita T, Takeuchi T, Fukuda T, Tsujiguchi M, Saburi T, Oshima R, et al. *Appl Phys Lett* 2000;77:1502.
- [12] Wuttig M, Li J, Craciunescu C. *Scripta Mater* 2001;44:2393.
- [13] Oikawa K, Ota T, Ohmori T, Tanaka Y, Morito H, Fujita A, et al. *Appl Phys Lett* 2002;81:5201.
- [14] Kainuma R, Gejima F, Sutou Y, Ohnuma I, Ishida K. *Mater Trans JIM* 2000;41:943.
- [15] Likhachev AA, Ullakko K. *Phys Lett A* 2000;275:142.
- [16] Heczko O, Jurek K, Ullakko K. *J Magn Magn Mater* 2001;226-230:996.
- [17] Heczko O, Straka L. *J Appl Phys* 2003;94:7139.
- [18] Marioni MA, O’Handley RC, Allen SM. *Appl Phys Lett* 2003;83:3966.
- [19] Enkovaara J, Ayuela A, Zayak AT, Entel P, Nordström L, Dube M, et al. *Mat Sci Eng A – Struct* 2004;378:52.
- [20] Zhang JX, Chen LQ. *Philos Mag Lett* 2005;85:533.
- [21] Kiang J, Tong L. *J Magn Magn Mater* 2005;292:394.
- [22] Kiefer B, Lagoudas DC. *Philos Mag* 2005;85:4289.
- [23] Ma YF, Li JY. *Acta Mater* 2007;55:3261.
- [24] Armstrong JN, Sullivan MR, Romancer ML, Chernenko VA, Chopra HD. *J Appl Phys* 2008;103:023905.
- [25] O’Handley RC. *J Appl Phys* 1998;83:3263.
- [26] Murray SJ, O’Handley RC, Allen SM. *J Appl Phys* 2001;89:1295.
- [27] Mullner P, Chernenko VA, Wollgarten M, Kostorz G. *J Appl Phys* 2002;92:6708.
- [28] Ma YF, Li JY. *Appl Phys Lett* 2007;90:172504.
- [29] Li JY, Ma YF. *Mech Mater* 2008;40:1022.
- [30] Couch RN, Chopra I. *Smart Mater Struct* 2007;16:S11.
- [31] Straka L, Heczko O. *IEEE Trans Magn* 2003;39:3402.
- [32] Straka L, Heczko O, Hanninen H. *Acta Mater* 2008;56:5492.
- [33] Likhachev AA, Ullakko K. *Eur Phys J B* 2000;14:263.
- [34] DeSimone A, James RD. *J Mech Phys Solids* 2002;50:283.
- [35] Liang Y, Wada T, Kato H, Tagawa T, Taya M, Mori T. *Mat Sci Eng A – Struct* 2002;338:89.
- [36] Marioni MA, O’Handley RC, Allen SM. *J Appl Phys* 2002;91:7807.
- [37] Glavatska NI, Rudenko AA, Glavatskiy IN, L’vov VA. *J Magn Magn Mater* 2003;265:142.
- [38] DeSimone A, James RD. *J Phys Iv* 2003;112:969.
- [39] Likhachev AA, Sozinov A, Ullakko K. *Mater Sci Eng A – Struct* 2004;378:513.
- [40] Liang YC, Kato H, Taya M. *Mech Mater* 2006;38:564.
- [41] Landis CM. *J Mech Phys Solids* 2008;56:3059.
- [42] Onisan AT, Bogdanov AN, Röbler UK. *Acta Mater* 2010;58:4378.
- [43] Koyama T, Onodera H. *Mater Trans* 2003;44:2503.
- [44] Bouville M, Ahluwalia R. *Acta Mater* 2008;56:3558.
- [45] Wu PP, Ma XQ, Zhang JX, Chen LQ. *J Appl Phys* 2008;104:073906.
- [46] Jin YM. *Acta Mater* 2009;57:2488.
- [47] Shu YC, Yen JH. *Appl Phys Lett* 2007;91:021908.
- [48] Shu YC, Yen JH. *Acta Mater* 2008;56:3969.
- [49] Yang L, Dayal K. *Appl Phys Lett* 2010;96:081916.
- [50] Lei CH, Li LJ, Shu YC, Li JY. *Appl Phys Lett* 2010;96:141910.
- [51] Shu YC, Yen JH, Chen HZ, Li JY, Li LJ. *Appl Phys Lett* 2008;92:052909.
- [52] Zhang YH, Li JY, Fang DN. *J Appl Phys* 2010;107:034107.
- [53] Li LJ, Li JY, Shu YC, Chen HZ, Yen JH. *Appl Phys Lett* 2008;92:172504.
- [54] Li LJ, Li JY, Shu YC, Yen JH. *Appl Phys Lett* 2008;93:192506.
- [55] Li LJ, Yang Y, Shu YC, Li JY. *J Mech Phys Solids* 2010;58:1613.
- [56] Chen LQ. *Annu Rev Mater Res* 2002;32:113.
- [57] Bhattacharya K. *Continuum Mech Therm* 1993;5:205.
- [58] Li JY, Liu D. *J Mech Phys Solids* 2004;52:1719.
- [59] Tsou NT, Huber JE. *Continuum Mech Therm* 2010;22:203.
- [60] Shu YC, Lin MP, Wu KC. *Mech Mater* 2004;36:975.
- [61] Landau L, Lifshitz E. *Phys Z Sowjetunion* 1935;8:153.
- [62] Gilbert T. *IEEE Trans Magn* 2004;40:3443.
- [63] Brown WF. *Micromagnetics*. New York: Wesley; 1963.
- [64] Zhang W, Bhattacharya K. *Acta Mater* 2005;53:185.
- [65] Zhang W, Bhattacharya K. *Acta Mater* 2005;53:199.